Optics & Laser Technology 176 (2024) 111001

Contents lists available at ScienceDirect

Optics and Laser Technology

journal homepage: www.elsevier.com/locate/optlastec

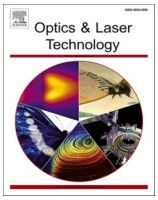

Full length article

Superlens-Assisted laser nanostructuring of Long Period optical fiber Gratings (LPGs) for enhanced refractive index sensing

Yiduo Chen [a], Liyang Yue [a], Xibin Yang [b,*], Charlotte L Jones [a], Zengbo Wang [a,*]

[a] School of Computer Science and Engineering, Bangor University, Dean Street, Bangor, Gwynedd LL57 1UT, UK
[b] Suzhou Institute of Biomedical Engineering and Technology, Chinese Academy of Sciences, Suzhou, Jiangsu 215163, China

ARTICLE INFO

Keywords:
Long period fiber grating
Superlens
Nanostructuring
Sensitivity

ABSTRACT

We introduce an innovative approach to enhance refractive index sensing utilizing Long Period Optical Fiber Gratings (LPGs) processed through microsphere-assisted superlens laser nanostructuring technology. This method involves the self-assembly of a silica microsphere monolayer on the outer surface of LPGs, followed by pulsed laser irradiation to create nanoholes (with a diameter of 300–500 nm) on the surface, for forming the nanohole-structured LPGs (NS-LPGs). The sensing capabilities of NS-LPGs, featuring two different nanohole densities (5 % and 7.9 %), were experimentally evaluated in sucrose and glycerin solutions. The results revealed a notable improvement in sensitivity, with increases of 16.08 % and 19.57 %, respectively, compared to conventional LPGs. This suggests that higher nanohole density contributes to greater enhancement in refractive index sensing. Furthermore, the permanent nanohole structures showed improved durability and lifespan in various environments compared to surface-coating-based LPGs. Further enhancements can be achieved by refining the nanostructuring density and controlling the dimensions of the nanoholes.

1. Introduction

Over the past few decades, we have witnessed significant growth and prominence of optical fiber grating sensors in various fields, including pharmacy, life sciences, security, food industry, and environmental monitoring. The development of optical fiber sensing technology is driven by its recognized advantages, such as its compact size, lightweight nature, immunity to electromagnetic interference, exceptional sensitivity, real-time monitoring capabilities, and the ability to multiplex [1–4], etc. Optical fiber grating sensors, as an important category of optical fiber sensors including Fiber Bragg Grating (FBG) and Long-period Grating (LPG) sensors, are based on the fundamental principle of leveraging evanescent fields created by the propagation of light within fiber-based devices and their interaction with the surrounding environment and media [5]. In the aspect of applications, FBGs are normally used for temperature and strain sensing, and LPGs work for refractive index sensing and monitoring of chemical processes most of the time [6]. The LPG gratings consist of periodic changes in the refractive index (RI) of fiber core, causing coupling between the core mode and co-propagating cladding modes and the resonance bands in the transmission spectrum. Each resonance band corresponds to a different cladding mode and offers varying sensitivity to environmental changes [7]. The RI sensitivity of LPGs is determined by the effective RI of the cladding modes. This effectiveness, in turn, depends on the contrast between the RIs of the cladding and the surrounding medium. Typically, the highest sensitivity of LPGs is achieved when the RI of the surrounding medium closely matches that of the cladding [8].

Various technologies have been employed to enhance the RI sensitivity of LPG sensors. These include the deposition of uniform thin-film coatings, such as PVA (Poly(vinyl alcohol)) [9], PDMS (Polydimethylsiloxane) [10], polyimide [11], graphene [12], graphene oxide [13], and Zn/ZnO [14], as well as nanoparticle coatings [15–17], and nanoparticle-embedded composite coatings [18,19]. Among the various methods for applying coatings to LPGs, the Layer-by-Layer technique is notable due to its outstanding capability to precisely control both the thickness and composition of nanoparticles in the resulting thin films. This versatile method enables the monitoring of a wide range of substances, including ethanol [20], ammonia [21], and low molecular analytes [22].

In this study, we propose a novel approach to enhance the RI sensitivity of LPG sensors. This involves employing the technology of direct laser nanostructuring of the surfaces of LPGs, assisted by

* Corresponding authors.
E-mail addresses: yangxb@sibet.ac.cn (X. Yang), z.wang@bangor.ac.uk (Z. Wang).

https://doi.org/10.1016/j.optlastec.2024.111001
Received 30 November 2023; Received in revised form 5 March 2024; Accepted 8 April 2024

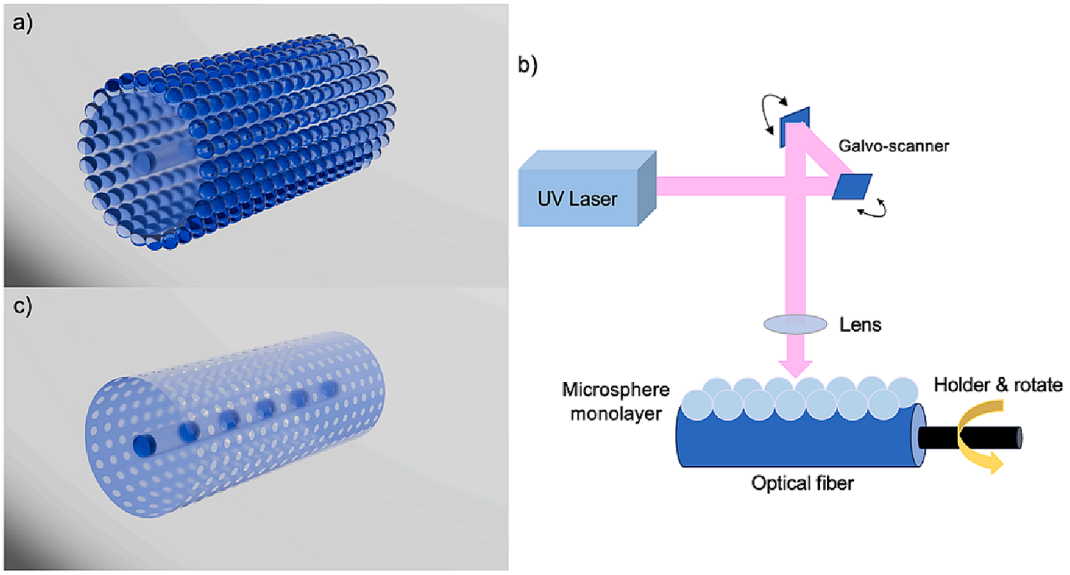

Fig. 1. Schematic of the experimental processes. a) Microsphere coating on LPG, b) Laser processing, c) Nanoholes fabricated on LPG.

microsphere superlenses that are coated onto the LPG surfaces. This results in the formation of nanohole-structured LPGs (NS-LPGs). The use of microsphere lenses as optical superlenses for nanoscale sub-wavelength patterning, imaging, and sensing has been an active research area since 2000 [23]. The patterning resolutions of 80–400 nm and imaging resolutions of 45–100 nm were reported in the literature [24–26], but no reports exist on microsphere-assisted nanostructuring of the fiber surface of LPG sensors to create NS-LPG sensors. In our experiments, we used a dip coating technique to apply a monolayer of silica microspheres across the entire surface of the optical fiber [27]. Subsequently, a pulsed UV laser system was used to ablate nanoholes on the surface of the fiber. The microsphere monolayer act as a focusing lens array, enabling the creation of numerous nanoholes. The RI sensing performance of the fabricated NS-LPGs were tested in both sucrose and glycerin solutions, and their efficiencies were compared with those obtained by standard LPG sensors. Our results indicated that the NS-LPG sensor can deliver higher sensitivity than the conventional LPG sensor. Also, we investigated the influences of nanohole density on sensing performance, finding that higher nanohole density can further improve sensitivity of NS-LPG.

2. Fabrication & experiment

2.1. Materials

Chemicals: Chemical reagents were sourced from established suppliers: Potassium hydroxide (KOH, 56.11 g/mol), poly(diallyl dimethylammonium chloride) (PDDA, 200 k-350 k molecular weight, 20 wt% in water), high-purity sucrose (≥99.5 %), and glycerol (≥99.5 %) were all obtained from Sigma-Aldrich (UK). Deionized (DI) water used in the experiments was from Thermo Fisher Scientific Inc. (UK). Different concentration solutions were prepared with DI water, and reagents were used as received, without further purification.

Microspheres: Colloidal silica microspheres with a diameter of 1 μm, a concentration of 50 mg/ml, and a coefficient of variation (CV) less than 3 % were procured from ALPHA Nanotech Inc. (United Kingdom).

LPGs: Long Period Fiber Gratings with a cladding diameter of 125 μm, core diameter of 8.2 μm, grating length of 20 mm, and grating period of 550 μm were sourced from oeMarket (Australia). These were fabricated from single-mode fiber (SMF-28).

2.2. Deposition of microsphere monolayer

The dip coating method was used to deposit a silica microsphere monolayer onto the LPG surface, using the Type G Ossila Dip Coater from Ossila, UK. The solutions included 5 wt% ethanolic KOH (ethanol/water = 3:2 v/v), 10 wt% PDDA in DI water, and 10 wt% silica microspheres in DI water. The LPG was attached to a dip coater holder, and then rinsed and cleaned with DI water and ethanol, respectively. It was immersed in the 5 wt% KOH solution for 20 min to produce a negatively charged surface. This was followed by submersion in a 10 wt% PDDA solution for an additional 20 min, succeeded by the 10 wt% silica microspheres solution. After these steps, the LPG was air-dried at 50 ℃ for an hour using a hotplate (Fisher Scientific Heater) to facilitate the deposition of the silica microsphere monolayer [28–30] (Fig. 1a). The dip and withdrawal speeds were consistently set at 50 mm/min and 2 mm/min, respectively. The microsphere-coated LPG sample was characterized using an advanced optical microscope (Olympus DSX1000) and a laser confocal microscope (3D Measuring Laser Confocal Microscope OLS5000).

2.3. Nanohole generation

As previously mentioned, microspheres can function as superlenses, focusing light to sub-wavelength spot sizes [27,31,32]. In our experiments (Fig. 1), a pulsed UV nanosecond laser beam (Guoke Century Laser, GKD-C40C20B, power: 10-Watt, wavelength: 355 nm, pulse duration: 100 ns, repetition rate: 50 kHz, spot size: 50 μm) was directed onto the microsphere-coated LPG sample and precisely scanned across it using a Galvo scanner at a speed of 100 mm/s (Fig. 1b). Since the fiber is a cylindrical structure, to ensure processing of the entire surface of the Long Period Grating (LPG), the LPG sample needed to be rotated during

Table 1
List of samples.

Sample	Description	Hole Density, *D* (hole area/total surface area)
LPG0 (S1, S2)	Original, non-processed LPG. S1: LPG0 for single-pass S2: LPG0 for double-pass	0 %
LPG1	Single-pass processed LPG	5 %
LPG2	Double-pass processed LPG	7.9 %

laser processing, facilitated by a specially designed rotational holder. After the initial laser treatment, most microspheres were removed due to the thermal expansion of the substrate and the laser ablation process, which simultaneously led to the formation of nanoholes beneath the majority of the microspheres. To prepare for a second round of processing, it is essential to rinse off any residual particles and reapply the particles uniformly across the entire fiber surface before proceeding with another laser exposure. It is also important to mention that the laser power was carefully controlled at approximately 0.53 J/cm^2 to prevent damage to the LPG grating within the fiber areas not covered by microspheres. This assurance stems from laser exposure tests conducted on standard LPG samples before applying microsphere coatings, where consistent sensing performance was observed before and after laser exposure, indicating no damage to the grating. In the experiments, two sets of nanohole densities were compared: sample **LPG1** involved a single pass of microsphere deposition and laser processing, while sample **LPG2** experienced double passes of microsphere deposition and laser processing for a larger nanohole density. Although this process can be repeated to further increase nanohole density, our study focuses on single-pass and double-pass processing only. For simplifying comparison, the unprocessed original LPG sample was referred to as **LPG0**, as shown in Table 1. The nanostructured LPG samples were characterized using various imaging techniques, including dark field microscopy, scanning electron microscopy (SEM, Hitachi TM4000Plus) and atomic force microscopy (AFM, Veeco Dimension 3100/V).

2.4. Refractive index sensing

The RI of solutions varies with concentration, with distinct RIs for each solute [33]. LPG sensors detect RI shifts, especially within the range of the RIs of water between 1.33 and 1.46 which is slightly smaller than that of cladding. LPG sensitivity can increase as the ambient RI approaches the RI of the cladding [34]. The laser-processed NS-LPGs are used to test the RIs of the solutions of varying concentrations of sucrose (0–70 wt%) and glycerin (0–90 wt%) in this study.

Our experimental setup illustrated in Fig. 2, utilized a broadband light source (BBS, NKT Photonics SuperK COMPACT) connected to an optical spectrum analyzer (OSA, Anritsu MS9740B) via NKT Photonics SuperK Fiber Delivery. After each immersion, the LPG was cleaned and dried to ensure consistent readings and prevent contamination.

The response of the LPG is influenced by the RI of the surrounding material. These changes can tune the spectral output of LPG, as the wavelengths of light attenuation depend on the effective RI of the cladding mode [8]. The LPG transfers of light from the core to specific cladding modes. Within the cladding, light diminishes due to scattering, leading to observable loss bands in the core output [35].

3. Results and discussion

3.1. Morphology of microsphere-coated LPG

Fig. 3 presents a detailed analysis of the surface morphology of LPGs coated with a monolayer of silica microspheres. Dark field optical images in Fig. 3a emphasize the efficient alignment and uniform distribution of microspheres across the fiber surface. The coating process achieved extensive coverage with approximately 95 % of the surface area of the fiber. In Fig. 3b, the 3D confocal image illustrates the arrangement of microspheres on the curved surface of the LPG. Notably, the monolayer of the microspheres exhibits consistency of the uniform coverage across the entire curved surface of the LPG, rather than any irregular distribution. Fig. 3c provides a close view of the monolayer-coated LPG, revealing the silica particles with the diameter of 1000 nm. This detailed view clearly demonstrates the silica microparticles arranged in a hexagonal honeycomb pattern, despite defects that could exist within them.

3.2. Morphology of nanostructured LPG

Fig. 4 illustrates the surface morphologies of LPG1 and LPG2 samples, following superlens-assisted laser nanostructuring for single-pass and double-pass, respectively. Nanoholes are clearly visible in dark-field optical microscopy (Fig. 4a). The zoomed SEM (Fig. 4b) and AFM images (Fig. 4c-d) reveal that these nanoholes are in the circular shape, with the diameters ranging from 300 to 500 nm and the depths ranging from 60 to 120 nm. Compared to Fig. 3, the patterns depicted in Fig. 4 demonstrate a notable increase in size variation and the presence of more defects. This disparity primarily stems from the laser processing procedure rather than the quality of the microsphere array. Firstly, the use of a non-flat top Gaussian beam results in particles within the spot being exposed to varying energy levels. Secondly, fluctuations in the temporal output of the laser energy during experimentation may influence the generation of nanoholes. Moreover, the curved surface of the fiber impacts how laser energy is transmitted from the microsphere to the substrate at different surface points, consequently affecting nanohole quality. To mitigate these issues, employing a uniform laser beam, such as a flat-top beam or a highly defocused Gaussian beam, is recommended to enhance nanohole quality and minimize defects in subsequent iterations of the process.

Comparing the samples in LPG1 and LPG2, it is observed that the double-pass processing results in higher nanohole densities. The calculated nanohole densities, defined as a ratio of the area with the generated nanoholes to the total surface area of the fiber, are approximately 5 % for the LPG1 sample and 7.9 % for the LPG2 sample. As noted earlier, after the initial laser processing pass, most microspheres on the fiber surface are ejected. Therefore, rinsing and reapplying them across the entire fiber surface before subsequent laser exposure rounds are crucial. This may lead to varied particle positions, causing uneven distribution and overlapping of resulting nanoholes (see LPG2 in Fig. 4c), but effectively increases nanohole density. Further density enhancement through repeated processing falls outside this study's scope but deserves future exploration.

3.3. RI sensitivity measurement

In a series of experiments, LPG1 with a 5 % nanohole density was exposed to sucrose aqueous solutions with the concentration ranging from 0 % to 70 % (DI water). Fig. 5a shows a significant red shift of 480 pm in the ambient air after nanohole structuring. The overall peak shift increased from 7.05 nm (unprocessed) to 8.16 nm (structured with nanoholes), representing a 15.7 % total shift increase (Fig. 5b-c). For LPG2, featuring double-pass nanostructuring with a 7.9 % nanohole density, the experiments involved the glycerin aqueous solutions with the concentration ranging from 0 % to 90 %. Fig. 5d demonstrates a red shift of 530 pm in the ambient air following nanohole structuring. The total peak shift increased from 8.79 nm (unprocessed) to 10.70 nm, indicating a 21.7 % total shift increase (Fig. 5e-f).

The red shifts of the peaks are attributed to the laser-generated nanoholes on the fiber, which lead to an increased surface contact area with enhanced light coupling between the cladding and the sensing medium. This will be considered in our model below, which differs from the classical model that uses a reduced cladding diameter [36,37].

The relationship between the solution weight ratio and RI for both sucrose and glycerin aqueous solutions is shown in Fig. 6a, displaying linear characteristics in line with the results in [33]. Fig. 6b & 6c presents the shifted peak locations of two LPGs, indicating their response to different solution concentrations before and after nanohole structuring. The slopes of these curves represent RI sensitivity, a critical sensing parameter that improves as the surrounding RI approaches the cladding material's RI [34]. The RI sensitivity is defined by the slope which is calculated by delta wavelength / delta weight ratio, giving a non-linear relationship. As an example, the sensitivity of LPG2 under glycerin concentration between 70 % and 80 % is 281 pm/% shown in Fig. 6 c.

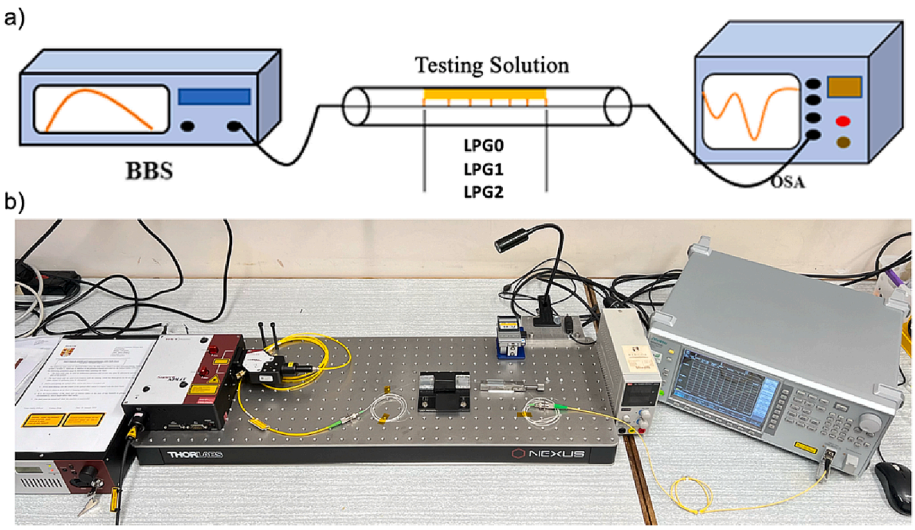

Fig. 2. Experimental setup for sensing testing. (a) Schematic representation, (b) Photograph of the setup.

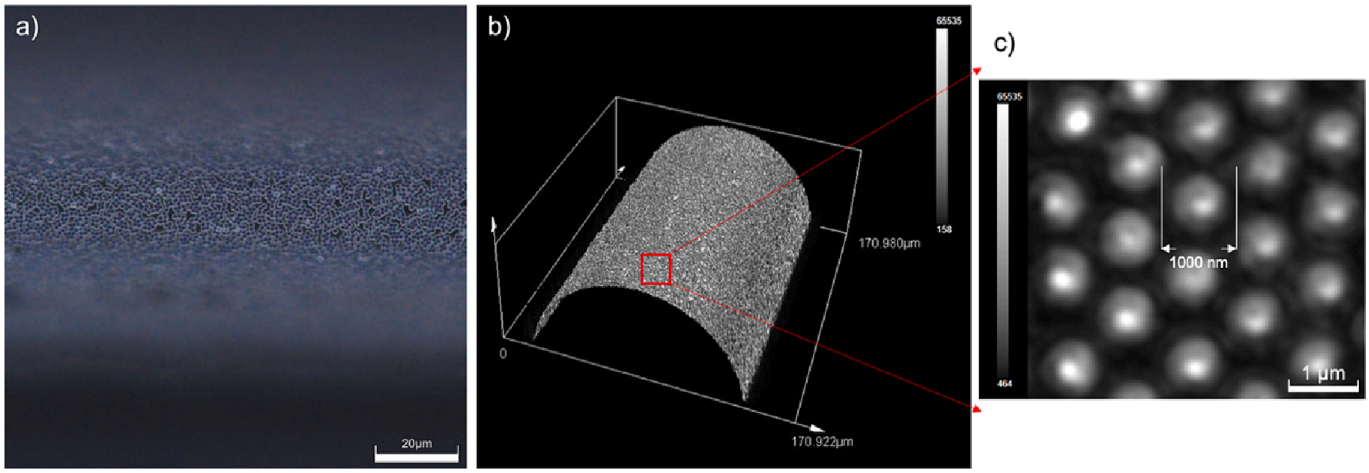

Fig. 3. Microscopic images of the microsphere-coated LPG surface. a) Dark field optical image, b) 3D confocal image of the curved surface coated with microspheres, and c) Magnified view of the microsphere array from (b).

The results of both LPG1 and LPG2 samples clearly demonstrate an improvement in slope, reflecting enhanced sensitivity after nanostructuring. The results also demonstrate that nanostructured LPG1 and LPG2 samples exhibit higher sensitivity compared to their original counterparts, as depicted in Fig. 7a and Fig. 7b, respectively. LPG1 shows the most significant sensitivity enhancement at 26.32 % within the 35–40 % sucrose weight ratio range (Fig. 7a), indicating an optimal concentration for maximum interaction between the cladding and the sensing medium. Also, Fig. 7b illustrates that LPG2's peak sensitivity increase is at 30.09 % in the presence of a 70–80 % glycerin weight ratio, suggesting a similar optimal concentration threshold for heightened response.

These experiments highlight the improved performance of nanostructured LPGs compared to the original unprocessed LPGs, with greater enhancements observed in structures with higher nanohole density. The increased total peak shifts indicate the improved performance of nanostructured LPGs and their potential for various optical and sensing applications. Ongoing efforts are focused on refining methods to achieve even higher nanohole density samples, thereby further advancing the sensitivity of nanostructured LPGs in applications based on the RI measurements. Moreover, the nanostructured surface may offer a novel avenue for interacting with sensing samples. For instance, virus particles or drug nanoparticles could potentially be entrapped within nanoholes, enabling detection.

We also conducted durability tests on the nanostructured LPGs in diverse environmental settings, exposing them to various chemicals such as acetone, methanol, and xylene, as well as temperatures ranging from −20 °C to 150 °C. Remarkably, throughout these tests, the nanohole structures maintained consistent sensing performance without noticeable degradation. In contrast, polymer-coated LPGs (e.g. PVA, PDMS) were found to be susceptible to the aforementioned tests, with the coating either being removed, damaged, or experiencing degraded sensing performance. This underscores the superior durability and extended lifespan of the permanent nanohole structures compared to surface-coating-based LPGs.

3.4. Modelling and simulation

To advance the understanding of the sensitivity characteristics of nanostructured Long Period Gratings (LPGs), we have refined an existing MATLAB computational model based on the coupled mode theory relevant to optical fiber waveguides [36,37]. This enhanced model, named the 'K2-model', accurately computes the transmission spectra for LPGs, facilitating a comprehensive investigation into the correlation between spectral peak shifts within nanostructured LPG waveguides and the dynamic refractive index (RI) changes in the surrounding medium.

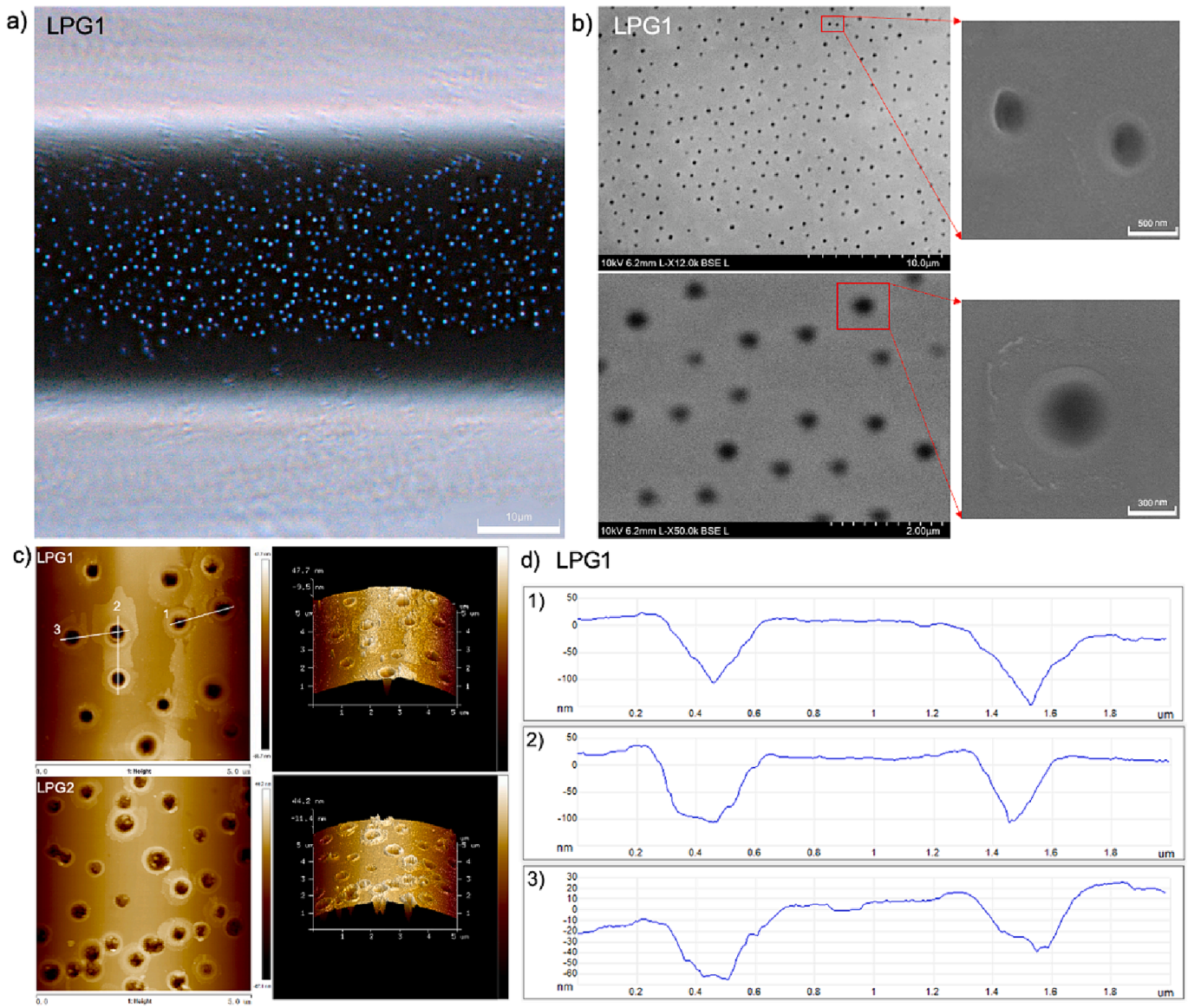

Fig. 4. Surface morphologies of processed LPG1 and LPG2 samples. a) Dark-field optical image of LPG1 sample. b) SEM image LPG1 sample, c) AFM images of LPG1 and LPG2 samples, d) depth profile of the LPG1 sample in c.

The model expresses the LPG transmission as follows:

$$T = cos^2\left(\sqrt{K_2^2 + K_1^2} \bullet L\right) + (K_1^2/(K_1^2 + K_2^2)) \bullet sin^2\left(\sqrt{K_2^2 + K_1^2} \bullet L\right) \quad (1)$$

In this expression, $K_1 = \delta + ½\,\kappa_1$, with δ as the self-detuning coefficient as outlined in reference [38[, and $K_2 = \alpha\,\kappa_2$, where α is the newly introduced parameter for this work termed the 'κ_2 enhancement factor'. K_1 and κ_2 are coupling coefficients of core and cladding, respectively (see Fig. 8a). The term L denotes the grating length. The 'κ_2 enhancement factor', α, is the principal modification to the existing model in [36]. This factor is a measure of the nanohole density (D) and the light scattering efficiency (S) by the nanoholes at the cladding/medium interface, and is given by the relationship:

$$\alpha = 1 + S{\cdot}D \quad (2)$$

The integration of α is vital as it captures the primary effect we observed in nanostructured LPGs. For our analysis, S is estimated at 1.01, with D at 5 % for LPG1 and 7.9 % for LPG2. The simulation replicates the parameters of the experimental LPGs, with a cladding diameter of 125 μm, core diameter of 8.2 μm, grating length of 20 mm, and a grating period of 550 μm. Particular attention is given to the peak with the highest sensitivity to RI changes, which is emphasized by the nanostructured surface.

Fig. 9a & 9d depict the simulated peak shifts for the original, unprocessed LPG0 sample. The total peak shift spans 8.14 nm as the RI varies from 1.0 to 1.445, serving as the baseline for subsequent comparisons with processed samples. During the single-pass nanostructuring model of the LPG1 sample, nanoholes were generated at a density of 5 %, leading to a 500 pm redshift of the transmission peaks in air compared to the LPG0 sample under the same conditions. Over the refractive index range from 1.0 to 1.445, the cumulative shift amounted to 9.44 nm for the LPG1 sample, indicating a 15.97 % increase compared to the unprocessed LPG0 sample, as illustrated in Fig. 9b and 9e. Aligned with experimental results, a 480 pm red-shift and a 16.08 % enhancement in shift was observed. Similarly, for the LPG2 sample subjected to double-pass nanostructuring model, nanoholes were generated at a density of 7.9 %, resulting in a 570 pm redshift of the peak wavelength in an air environment. The total shift reached 9.63 nm, reflecting an 18.30 % increase compared to the unprocessed LPG over the entire refractive

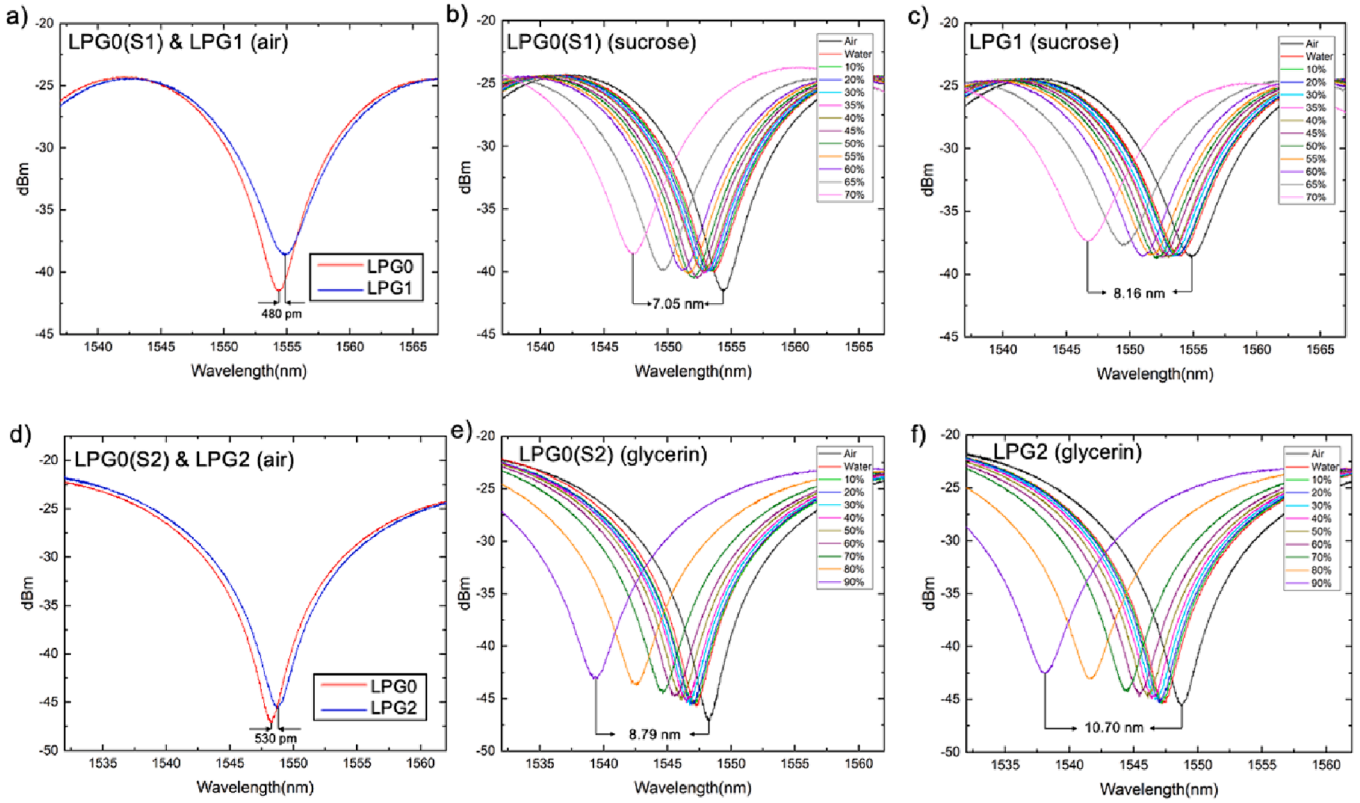

Fig. 5. Transmission spectrum of (a) LPG1 in air, before and after nanostructuring, (b-c) LPG1 sensing of sucrose solution at various concentrations before and after nanostructuring, (d) LPG2 in air, before and after nanostructuring, (e-f) LPG2 sensing of glycerin solution at various concentrations before and after nanostructuring.

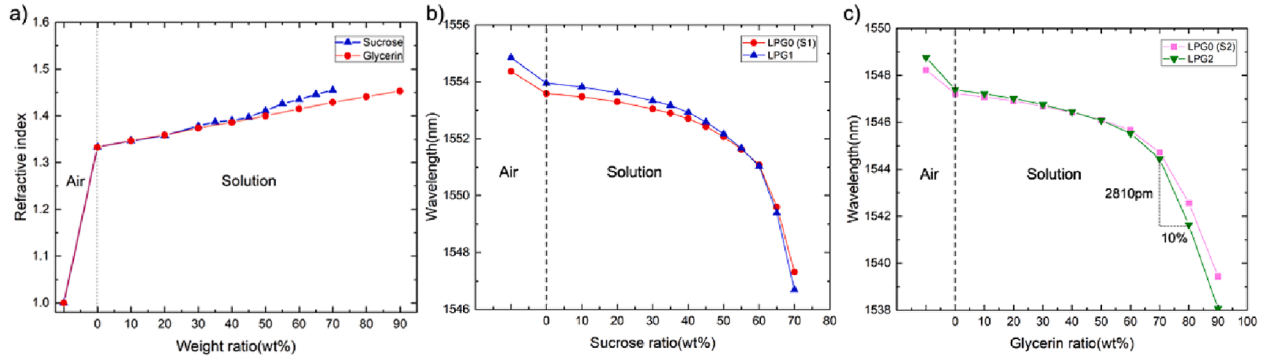

Fig. 6. (a) Relationships between solution weight ratio and refractive index, (b) shifted peak locations of LPG0 (S1) & LPG1 at varying solution concentrations, (c) shifted peak locations of LPG0 (S2) & LPG2 at varying solution concentrations.

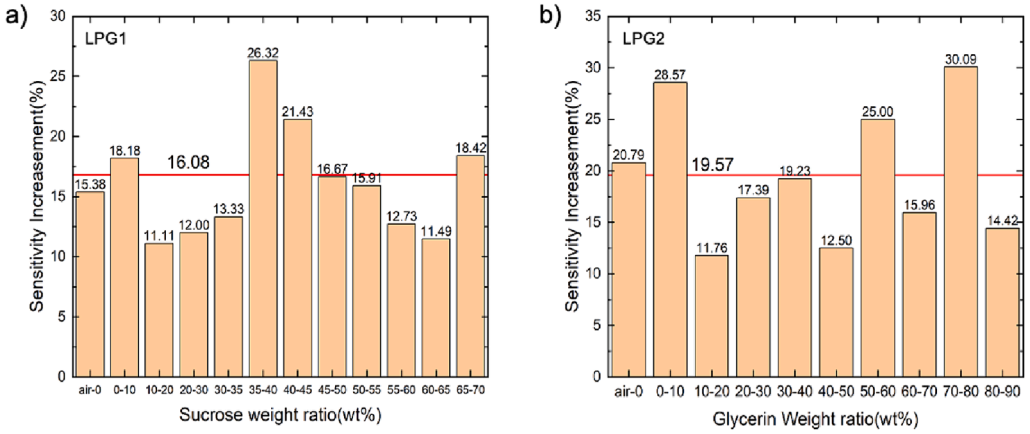

Fig. 7. Sensitivity increase of (a) LPG1 for sucrose solution concentration interval, (b) LPG2 for glycerin solution concentration interval.

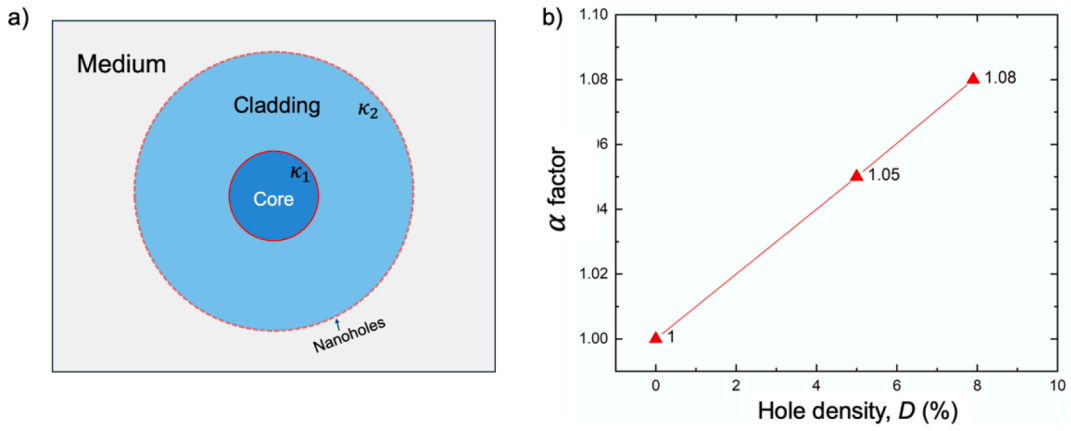

Fig. 8. (a) Schematic of modelling geometry (not to scale) and (b) α, the enhancement factor of K_2, as a function of hole density.

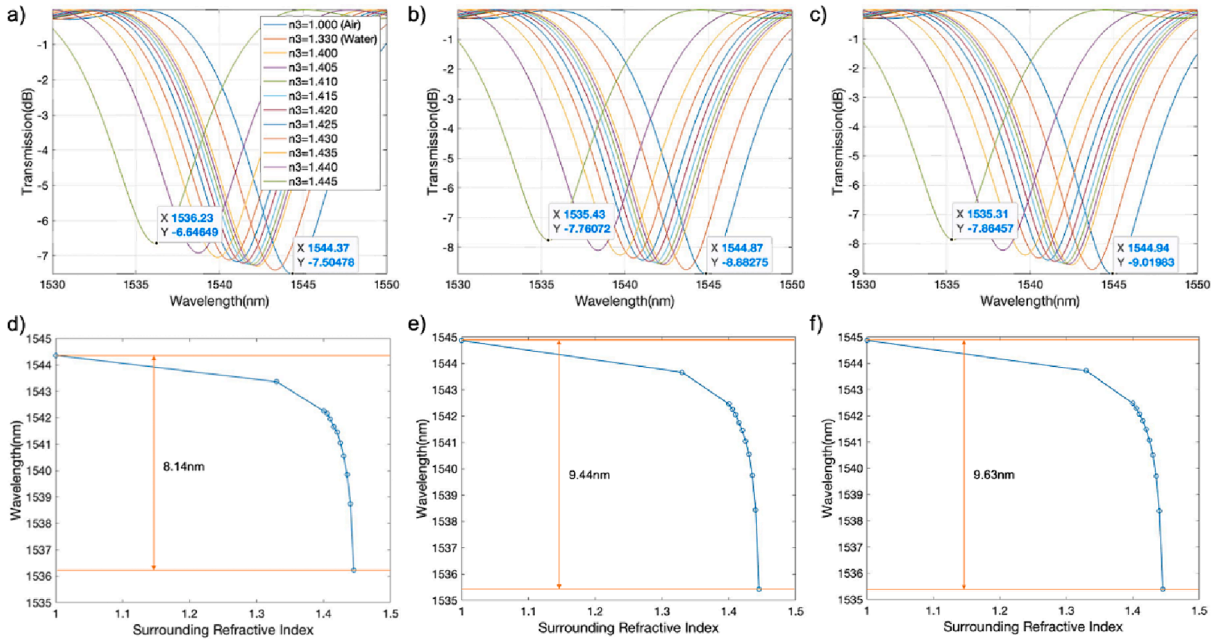

Fig. 9. Simulated transmission curves and corresponding peak wavelength as function of RI ranging from 1.0 to 1.445 for (a,d) LPG0 (original), (b,e) LPG1 (5% hole density) and (c,f) LPG2 (7.9% hole density) samples, respectively.

index range, which is also in line with experimental results showing a 530 pm redshift and a 19.57 % increase in shift.

In summary, our proposed 'K2-model' effectively elucidates the improved sensing performance and fundamental physics of nanostructured holes on LPG sensors. The increased surface area provided by nanoholes enhances the coupling between the cladding layer and the sensing medium, resulting in the observed peak red-shift effect (theoretical 500–570 pm redshift versus experimental 480–530 pm redshift) and enhanced sensitivity (theoretical 15.97–18.30 % versus experimental 16.08–19.57 %).

4. Conclusion

In conclusion, our study presents an innovative approach to enhance the sensitivity of Long Period Optical Fiber Gratings (LPGs) for refractive index sensing. This enhancement is achieved by creating nanohole-structured LPGs (NS-LPGs) using a novel microsphere-assisted superlens laser nanostructuring technology. Our experiments compared the NS-LPGs with different nanohole densities in sucrose and glycerin solutions. The results demonstrated a remarkable increase in sensitivity, with NS-LPGs showing enhancements of 16.08 % and 19.57 % in sucrose and glycerin solutions, respectively, compared to traditional LPGs. Higher nanohole density resulted in greater sensitivity improvements. Crucially, these nanohole structures provide exceptional durability by eliminating the problem of coating layer damage, effectively resolving common issues encountered with conventional surface-coated LPGs. Our research represents a significant advancement in LPG sensor technology, emphasizing the potential of surface nanostructuring to enhance refractive index sensing capabilities. This innovation holds promise for a wide range of practical applications.

Funding

Leverhulme Trust Fellowship (RF-2022–659); Royal Society (IEC\R2 \ 202,040 and IEC\R2\202178); National Key Research and Development Program of China (2021YFC2400100, zchj2022006L); National Natural Science Foundation of China (62375280); Basic Research Program of Suzhou (szs2020308, SJC2022009 , SSD2023010, SSD2023020; Youth Innovation Promotion Association of ACS (2023340).

CRediT authorship contribution statement

Yiduo Chen: Writing – original draft, Visualization, Methodology, Investigation, Data curation. **Liyang Yue:** Writing – review & editing, Validation, Methodology, Funding acquisition. **Xibin Yang:** Software, Validation, Writing – review & editing, Funding acquisition, Formal analysis, Methodology. **Charlotte L Jones:** Visualization, Methodology, Investigation. **Zengbo Wang:** Writing – review & editing, Supervision, Project administration, Funding acquisition, Conceptualization.

Declaration of competing interest

The authors declare that they have no known competing financial interests or personal relationships that could have appeared to influence the work reported in this paper.

Data availability

Data will be made available on request.

References

[1] B. Lee, Review of the present status of optical fiber sensors, Opt. Fiber Technol. 9 (2) (2003) 57–79.
[2] B. Culshaw, Optical fiber sensor technologies: opportunities and-perhaps-pitfalls, J. Lightwave Technol. 22 (1) (2004) 39.
[3] X. Fan, I.M. White, Optofluidic microsystems for chemical and biological analysis, Nat. Photonics 5 (10) (2011) 591–597.
[4] X.D. Wang, O.S. Wolfbeis, Fiber-optic chemical sensors and biosensors (2013–2015), Anal. Chem. 88 (1) (2016) 203–227.
[5] X. Shu, L. Zhang, I. Bennion, Sensitivity characteristics of long-period fiber gratings, J. Lightwave Technol. 20 (2) (2002) 255.
[6] G. Rego. A review of refractometric sensors based on long period fibre gratings. Sci. World J. (2013).
[7] V. Bhatia, A.M. Vengsarkar, Optical fiber long-period grating sensors, Opt. Lett. 21 (9) (1996) 692–694.
[8] Q. Shi, B.T. Kuhlmey, Optimization of photonic bandgap fiber long period grating refractive-index sensors, Opt. Commun. 282 (24) (2009) 4723–4728.
[9] T. Venugopalan, T. Sun, K.T.V. Grattan, Long period grating-based humidity sensor for potential structural health monitoring, Sens. Actuators, A 148 (1) (2008) 57–62.
[10] Q. Wang, C. Du, J. Zhang, R. Lv, Y. Zhao, Sensitivity-enhanced temperature sensor based on PDMS-coated long period fiber grating, Opt. Commun. 377 (2016) 89–93.
[11] L. Wang, N. Fang, Z. Huang, M. Abadie. Polyimide-coated fiber bragg grating sensors for humidity measurements. high performance polymers-polyimides based-from chemistry to applications (2012).
[12] W. Wei, J. Nong, G. Zhang, L. Tang, X. Jiang, N. Chen, Y. Zhu, Graphene-based long-period fiber grating surface plasmon resonance sensor for high-sensitivity gas sensing, Sensors 17 (1) (2016) 2.
[13] C. Liu, Q. Cai, B. Xu, W. Zhu, L. Zhang, J. Zhao, X. Chen, Graphene oxide functionalized long period grating for ultrasensitive label-free immunosensing, Biosens. Bioelectron. 94 (2017) 200–206.
[14] Y. Li, Y. Wang, C. Wen, Temperature and strain sensing properties of the zinc coated FBG, Optik 127 (16) (2016) 6463–6469.
[15] A. Abdelghani, J.M. Chovelon, N. Jaffrezic-Renault, M. Lacroix, H. Gagnaire, C. Veillas, V. Matejec, Optical fibre sensor coated with porous silica layers for gas and chemical vapour detection, Sens. Actuators B 44 (1–3) (1997) 495–498.
[16] A. Urrutia, J. Goicoechea, A.L. Ricchiuti, D. Barrera, S. Sales, F.J. Arregui, Simultaneous measurement of humidity and temperature based on a partially coated optical fiber long period grating, Sens. Actuators B 227 (2016) 135–141.
[17] Y.C. Tan, W.B. Ji, V. Mamidala, K.K. Chow, S.C. Tjin, Carbon-nanotube-deposited long period fiber grating for continuous refractive index sensor applications, Sens. Actuators B 196 (2014) 260–264.
[18] D. Viegas, J. Goicoechea, J.L. Santos, F.M. Araújo, L.A. Ferreira, F.J. Arregui, I. R. Matias, Sensitivity improvement of a humidity sensor based on silica nanospheres on a long-period fiber grating, Sensors 9 (1) (2009) 519–527.
[19] S. Lepinay, A. Staff, A. Ianoul, J. Albert, Improved detection limits of protein optical fiber biosensors coated with gold nanoparticles, Biosens. Bioelectron. 52 (2014) 337–344.
[20] M. Konstantaki, A. Klini, D. Anglos, S. Pissadakis, An ethanol vapor detection probe based on a ZnO nanorod coated optical fiber long period grating, Opt. Express 20 (8) (2012) 8472–8484.
[21] S. Korposh, R. Selyanchyn, W. Yasukochi, S.W. Lee, S.W. James, R.P. Tatam, Optical fibre long period grating with a nanoporous coating formed from silica nanoparticles for ammonia sensing in water, Mater. Chem. Phys. 133 (2–3) (2012) 784–792.
[22] R.Z. Yang, W.F. Dong, X. Meng, X.L. Zhang, Y.L. Sun, Y.W. Hao, H.B. Sun, Nanoporous TiO2/polyion thin-film-coated long-period grating sensors for the direct measurement of low-molecular-weight analytes, Langmuir 28 (23) (2012) 8814–8821.
[23] Y.F. Lu, L. Zhang, W.D. Song, Y.W. Zheng, B.S. Luk'Yanchuk, Laser writing of a subwavelength structure on silicon (100) surfaces with particle-enhanced optical irradiation, J. Exp. Theor. Phys. Lett. 72 (2000) 457–459.
[24] Z.B. Wang, M.H. Hong, B.S. Luk 'yanchuk, S.M. Huang, Q.F. Wang, L.P. Shi, T. C. Chong, Parallel nanostructuring of GeSbTe film with particle mask, Appl. Phys. A 79 (2004) 1603–1606.
[25] Z. Wang, W. Guo, L. Li, B. Luk'Yanchuk, A. Khan, Z. Liu, Z. Chen, M. Hong, Optical virtual imaging at 50 nm lateral resolution with a white-light nanoscope, Nat. Commun. 2 (1) (2011) 218.
[26] V.N. Astratov, et al., Roadmap on label-free super-resolution imaging, Laser Photonics Rev. 2200029 (2023).
[27] I. Jasim, J. Liu, C. Zhu, M. Roman, J. Huang, E. Kinzel, M. Almasri, Microsphere photolithography patterned nanohole array on an optical fiber, IEEE Access 9 (2021) 32627–32633.
[28] S. Korposh, S.W. Lee, S.W. James, R.P. Tatam, Refractive index sensitivity of fibre-optic long period gratings coated with SiO2 nanoparticle mesoporous thin films, Meas. Sci. Technol. 22 (7) (2011) 075208.
[29] V. Lotito, T. Zambelli, Approaches to self-assembly of colloidal monolayers: a guide for nanotechnologists, Adv. Colloid Interface Sci. 246 (2017) 217–274.
[30] J. Hrubý, V.T. Santana, D. Kostiuk, M. Bouček, S. Lenz, M. Kern, P. Neugebauer, A graphene-based hybrid material with quantum bits prepared by the double langmuir-schaefer method, RSC Adv. 9 (42) (2019) 24066–24073.
[31] A. Khan, Z. Wang, M.A. Sheikh, D.J. Whitehead, L. Li, Parallel near-field optical micro/nanopatterning on curved surfaces by transported micro-particle lens arrays, J. Phys. D Appl. Phys. 43 (30) (2010) 305302.
[32] J. Liu, I. Jasim, T. Liu, J. Huang, E. Kinzel, M. Almasri, Off-axis microsphere photolithography patterned nanohole array and other structures on an optical fiber tip for glucose sensing, RSC Adv. 11 (42) (2021) 25912–25920.
[33] W.M. bin Mat Yunus, A. bin Abdul Rahman, Refractive index of solutions at high concentrations, Appl. Opt. 27 (16) (1988) 3341–3343.
[34] S.W. James, R.P. Tatam, Optical fibre long-period grating sensors: characteristics and application, Meas. Sci. Technol. 14 (5) (2003) R49.
[35] H.J. Patrick, A.D. Kersey, F. Bucholtz, Analysis of the response of long period fiber gratings to external index of refraction, J. Lightwave Technol. 16 (9) (1998) 1606.
[36] T. Erdogan, Fiber grating spectra, J. Lightwave Technol. 15 (8) (1997) 1277–1294.
[37] C.Y. Tsao, D.N. Payne, W.A. Gambling, Modal characteristics of three-layered optical fiber waveguides: a modified approach, JOSA A 6 (4) (1989) 555–563.
[38] S. Miao, X. Hu, Transmission spectrum simulation of long period fiber grating, J. Phys. Conf. Ser. 1549 (2) (2020) 022146.